

**Babes-Bolyai University
Faculty of Physics**

Doctoral Thesis Summary

**FABRICATION AND DEMONSTRATION OF
UNCONVENTIONAL PLASMONIC SUBSTRATES
TOWARDS SERS BIOSENSING APPLICATIONS**

By

Cosmin Ioan LEORDEAN

Scientific advisor

Prof. Univ. Dr. Simion AȘTILEAN

CLUJ-NAPOCA

2014

Table of content

Thesis outline	2
Chapter 1 Plasmonic nanostructures -based biosensors: General aspects	4
1.1 <i>Biosensor: Overview</i>	4
1.2 <i>Theoretical background</i>	4
1.2.1 <i>Surface plasmons</i>	4
1.2.2 <i>Utilization of plasmonic nanostructures in sensing applications</i>	5
1.3 <i>Fabrication methods of nanostructured substrates</i>	7
Chapter 2 FABRICATION OF NANOSTRUCTURED SUBSTRATES BASED ON GOLD NANOPARTICLES	8
2.1 <i>Fabrication of plasmonic substrate by assembling of gold nanoparticles</i>	8
2.1.1 <i>Drop-casting method</i>	8
2.1.2 <i>Chemical attachment method</i>	9
2.1.3 <i>Convective self-assembling method</i>	10
2.2 <i>SERS performance of nanostructured substrates</i>	11
2.3 <i>Application of plasmonic substrates in multi-analyte detection of biomolecules from biological fluids</i>	13
2.3.1 <i>Multi-analyte detection</i>	13
2.3.2 <i>Detection of urea trace in biological fluids</i>	14
Chapter 3 FABRICATION OF MICROPATTERNED NANOSTRUCTURATED SUBSTRATE FOR MULTIPLICATIVE ELECTROMAGNETIC SERS ENHANCEMENT	15
3.1. <i>Fabrication of periodically micro-structured gold nanoparticle films</i>	15
3.2 <i>Characterization of periodically micro-structured gold nanoparticle films</i>	16
3.2.1 <i>Morphological characterization</i>	16
3.2.2 <i>Optical characterization</i>	16
3.3 <i>Assessment of multiscale electromagnetic SERS enhancement</i>	17
3.3.1 <i>SERS performance</i>	17
3.3.2 <i>Spot to spot reproducibly, time stability and reutilization</i>	19
3.3.3 <i>Finite differences time domain (FDTD) simulations</i>	20
Chapter 4 FABRICATION OF ORDERED PLASMONIC SUBSTRATE FOR DETECTION AND QUANTITATIVE ANALYSIS USING SERS	21
4.1 <i>Two step fabrication process of pyramidal shaped substrate through nanoimprinting lithography</i> 21	
4.2 <i>Characterization of pyramidal-shaped plasmonic substrate</i>	22
4.2.1 <i>Morphological characterization</i>	22
4.2.2 <i>Optical characterization</i>	24
4.2.3 <i>Finite differences time domain (FDTD) simulations</i>	24
4.3 <i>Spectroscopic properties of pyramidal-shaped plasmonic substrate</i>	25
4.4 <i>Detection and quantitative analysis of urea molecules</i>	26
Chapter 5 FINAL CONCLUSIONS	28
References	29
List of publications	31

THESIS OUTLINE

Biosensors represent a market over US\$13 billion with application in medicine, pharmacy, food and process control, environmental monitoring, defense and security. The increasing healthcare costs together with consumer demand, enforce the development of a new generation of inexpensive wearable, integrated and less-invasive sensors amenable to mass production to support the maintenance of wellbeing, care of the elderly, pharmaceutical development and testing, and distributed diagnostics. Nanotechnology plays an increasingly important role in the development of biosensors. The sensitivity and performance of biosensors is being improved by using materials with nanoscale features for their construction. In this context, the fabrication of plasmonic nanostructures for development of biosensors represent an important challenge for researchers.

Chapter 1 an overview of plasmonic nanostructures – based biosensors, with highlight on the basic concepts of biosensors, in particular plasmonic biosensors, theoretical aspects regarding the effect of surface plasmons and different strategies used for the fabrication of nanostructured materials, such as top-down and bottom-up fabrication methods.

The following four chapters and contains the experimental results obtained during my PhD period at Nanobiophotonics Center of the Interdisciplinary Research Institute in Bio-Nano-Sciences from Babes-Bolyai University Cluj-Napoca Romania.

Chapter 2 presents three very simple strategies, based on the assembly of chemically synthesized gold nanoparticles (NPs), used to easily fabricate nanostructured plasmonic substrates with applicability in Surface Enhanced Raman Scattering (SERS) – based optical detection and identification of molecular species of biological or chemical interests, pollutants or warfare agents.

The employed strategies can be implemented in any laboratory, without the need of specialized equipment, for preparation of citrate-stabilized spherical gold NPs assemblies and consist in : (i) drop-coating method, which induces the assembly of colloids in so-called coffee rings, (ii) assembly of NPs onto chemically functionalized glass surfaces, which yields randomly assembled colloids and colloidal clusters and (iii) a simplified variant of convective self-assembly (CSA), based on water evaporation in a constrained geometry, which yields highly uniform strips of NPs. The SERS properties of the resulting colloidal assemblies are comparatively evaluated under multiple excitation lines with p-aminothiophenol (pATP) as a model Raman reporter. The NPs strips obtained by CSA prove to be SERS-active both in the visible and NIR spectral regions and possess a highly uniform SERS response as demonstrated by confocal SERS mapping. Further it is shown that the obtained NPs strips are effective for the detection of cytosine, a DNA component, and for multi-analyte SERS detection. These results, showing how an efficient SERS substrate can be obtained by a very simple assembly method from easy-to-synthesize colloidal gold NPs, can have an impact on the development of analytical SERS applications.

In **Chapter 3** is detailed the fabrication of periodically micropatterned films made of colloidal gold NPs, prepared by a self-assembly approach, without implying lithography procedures in order to demonstrate a cascaded, multiplicative electromagnetic enhancement effect in SERS. The multiplicative enhancement effect is obtained by combining surface plasmon near-field enhancement due to nanoscale features with far-field photonic coupling by periodic microscale features. The effect is observed for both internal Raman reporters (molecules attached to the Au colloids before their assembly) and external Raman probes (molecules adsorbed on the samples after film assembly). The ability of the patterned films for far-field light coupling is supported by reflectivity spectra, which present minima/maxima in the visible spectral range. The experimental results are confirmed by Finite-difference time-domain simulations of the electric field distribution. The fabricated dual-scale SERS substrates exhibit a good spot-to-spot reproducibility and time stability, as proved by the SERS response over a time scale longer than 1 month. The experimental demonstration of this cascaded electromagnetic enhancement effect contributes to a better understanding of SERS and can have a positive effect on the future design of SERS substrates. Moreover, such dual-scale colloidal films prepared by CSA can be of general interest for the broader field of NPs-based devices.

Chapter 4 is focused on emphasizing a simple approach for the fabrication of periodically ordered pyramidal-shaped metallic nanostructures and demonstrating their efficiency as SERS active substrates. The employed method is based on nanoimprint lithography and exploits the thermal properties of two classes of polymers, thermoplastics and hydrogels. During the heating process the thermoplastic polymers start to melt whereas the hydrogel polymers form a solid due to the evaporation of water molecules adsorbed during the dissolving process. Making use of this approach and a textured commercial DVD as the initial mold, highly ordered pyramidal-shaped nanostructures were successfully fabricated using. This technique represents a low-cost alternative to the classical lithography techniques, allowing the fabrication over large areas ($\sim \text{cm}^2$) of periodically ordered nanostructures in a controlled and reproducible manner.

The SERS efficiency of the fabricated substrate is demonstrated through the detection of urea molecules found in the fingerprint. In addition, due to the periodicity of the pyramidal-shaped structures, the fabricated substrate can be successfully employed to correlate the intensity of the specific SERS peak of urea with the molecules concentration, offering thus the possibility of developing a quantitative SERS renal sensor.

The final conclusions of my work are presented in **Chapter 5**.

This work was supported by “Investing in people” - Ph.D. scholarship, project co-financed by the Sectoral Operational Program for Human Resources Development 2007 – 2013, Contract nr. POSDRU/159/1.5/S/132400- “Young successful researchers – professional development in an international and interdisciplinary environment”, Babeş-Bolyai University, Cluj-Napoca, Romania.

CHAPTER 1

PLASMONIC NANOSTRUCTURES -BASED BIOSENSORS: GENERAL ASPECTS

1.1 Biosensor: Overview

The field of biosensor emerged in 1967, when Updike and Hicks publish in the Nature Journal the first device for detection of glucose (Updike and Hicks, 1967). From this starting point a wide range of biosensor technologies were developed with application in various fields like: food control (e.g. detection of food toxins), medical diagnostics (e.g. detection of disease markers) and environment monitoring (e.g. pollutants detection) (Turner, 2000). According to Union of Pure and Applied Chemistry a biosensor can be described as an analytical device or unit, used for the detection of an analyte that is associates to or integrates a biological component by a physico-chemical detector, namely a transducer (Turner, 2000). The components of a biosensor are schematically presented in Figure 1-1.

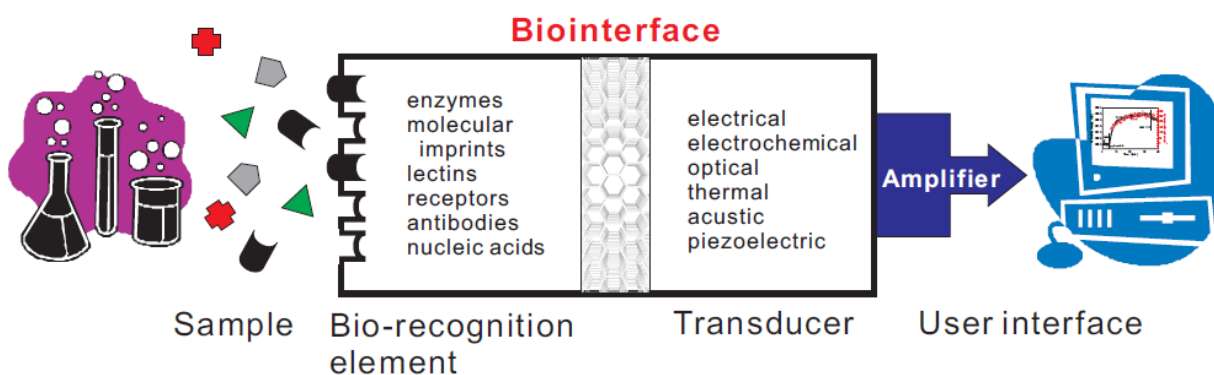


Figure 1-1: Schematic representation of a biosensor.

Depending on the bio-recognition element, biosensors can be classified into two major groups: catalytic-based and affinity-based biosensors. The transducer has the role of translating the recognition events (e.g. enzymatic catalysis or analyte capture) into a chemical or physical signal (e.g. electrical, electrochemical, optical, thermal, acoustic). Among the different types of optical biosensors developed over the last decade, those based on surface plasmonic effects became the most popular due to their high sensitivity, label-free and real-time detection of molecular bindings.

1.2 Theoretical background

1.2.1 Surface plasmons

In the last decade researchers are carried out an intense work in order to understand the plasmonic fundamentals and developing of plasmonic device based on nanostructures. In the field of nanophotonics, plasmonics represents a relative new direction that have as a ground state

properties of collective electron excitation, which are known also as *surface plasmons*, in films or nanostructure of noble metals (Au, Ag, Cu) (Kreibig and Vollmer, 1995; Raether, 1988). Researchers observed that surface plasmons can be found in different forms such as propagative electron density waves at the interfaces between a dielectric and a metallic layer or localized electron oscillation in metallic nanostructures or nanoparticles.

Surface plasmon polaritons (SPPs) can be described as electromagnetic waves that are propagating at the interface between metallic and dielectric media. In 1902, Prof. Robert W. Wood made the first observation of SPPs. In 1968 two teams of researchers, one led by Andreas Otto and other led by Erich Kretschmann and Heinz Rarther, demonstrated almost in the same time that by using an optical prism it is possible to achieve optical excitation of plasmons on metal films (Kretschmann and Raether, 1968; Otto, 1968).

Noble metal nanoparticles are known to have remarkable properties arise after the direct interaction between the incident light with the collective oscillation of the metal surface conductive electrons confined on metal nanoparticles, which are known as localized surface plasmons (LSPs). As a result of this interaction, noble metal nanoparticles will exhibit a strong absorption band in the UV-Vis region, which is not present in the bulk metal spectrum (Haynes and Van Duyne, 2001). This absorption band is known as localized surface plasmon resonance (LSPR). LSPR excitation results in wavelength-selective absorption with extremely large molar extinction coefficients $\sim 10^{11} \text{ cm}^{-1}$ (Jensen et al., 2000) resonant Rayleigh scattering (Michaels et al., 1999) with an efficiency equivalent to that of 10^6 fluorophores (Yguerabide and Yguerabide, 1998) and enhanced local electromagnetic fields near the surface of the nanoparticle (Zhang et al., 2006).

1.2.2 Utilization of plasmonic nanostructures in sensing applications

Optical biosensors based on plasmonic transducers represent a strong choice in non-labeling analysis of biomolecular interaction (Hall, 2001; Schuck, 1997). For example, by using a device based surface plasmon resonance (SPR) that work as a plasmonic transduction based on the excitation of surface plasmons on planar gold surfaces, environment changes has been identified by recording any changes what appears in the reflectivity spectra. The literature results demonstrate that using biosensors based on SPR investigation of binding molecules at very low concentration has been achieved.

In the case of metallic nanoparticles, the electromagnetic field has an operation mode very similar with the propagation of SPPs on a flat metallic film and enables the transduction of chemical binding events into a measurable wavelength shift of the extinction peak. Despite demonstrated efficiency of LSPR biosensors based on nanoparticles in laboratory (Coe et al., 2008; Liu et al., 2006), the fabrication of biosensor devices based nanoparticle-based LSPR still remains a difficult task and requires important improvements regarding spatial resolution, reproducibility and monodispersity in size and shape of metallic nanoparticles.

In comparison to LSPR based biosensors, Surface Enhanced Raman Scattering (SERS) based biosensors work by increasing the Raman signal of analyte molecules that are located very close or in contact with the surface of metallic nanostructures and interact with the SPR. Raman scattering is an inelastic process in which the incident photons are able to increase from or lose energy to the vibrational motion of the analyte molecules. The resulting spectrum of Raman scattering consist in a series of bands that are corresponding to vibrational or rotational transition specific to the structure of molecule, thus providing a very specific chemical “fingerprint” very useful for analyte identification. Despite the great advantage of high specificity, the Raman scattering process is a very weak phenomenon as only approximation 1 to 10^6 - 10^{10} photons are inelastically scattered (McCreery, 2000). Thus, by employing plasmonic nanostructures, with plasmon resonances located within the wavelength range used to excite Raman modes, researchers were able to detect chemical “fingerprint” of a single molecule due to increase the Raman signal up to 14 or 15 order of magnitude. The most dominant contribution in SERS has the so called electromagnetic mechanism (Figure 1-2).

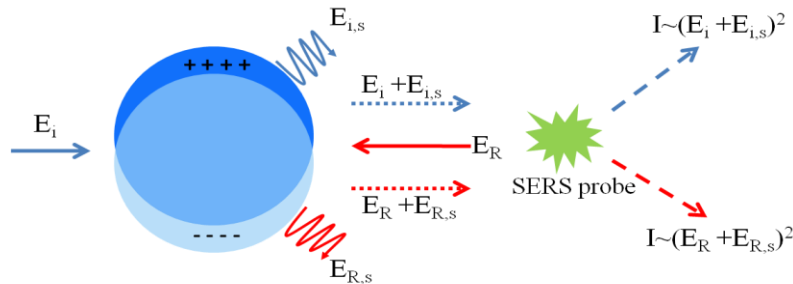


Figure 1-2: Schematic representation of the electromagnetic enhancement mechanism in SERS.

In the case that fluorophores are placed in close contact with metallic surface of nanostructures the interaction between the fluorophores electrons and strong plasmon field could change the fluorescence emission level by enhance or quench the emission. First who observe this metal-enhanced fluorescence (MEF) phenomenon was Drexhage et al. in 1974. The electric field felt by a fluorophore is affected by interaction of the incident light with the nearby metal surface and also by interaction of the fluorophore oscillating dipole with the metal surface. Furthermore, the fluorophores oscillating dipole induces a field in the metal. In fact, these interactions can increase or decrease the field incident on the fluorophore and increase or decrease the radiative decay rate.

Therefore the interaction between fluorophores and metallic nanostructure is attracting wide interest because of useful application as optical waveguides, biosensors and nonlinear optical materials (Noginov et al., 2005). In conclusion alongside the SERS the fluorescence enhancement effect presents significant applications protein detection (Aslan et al., 2005), drug discovery or immunoassays.

1.3 Fabrication methods of nanostructured substrates

In its broadest terms, nanoscale fabrication, or simply nanofabrication, refers to the design, construction and manipulation of materials having small dimensions that are typically in the range of 1 to 100 nm. The different nanofabrication methods are usually classified into two main categories: (1) bottom-up and (2) top-down.

The top-down approaches carve nanoscale structures by controlled removal of materials from larger or bulk solids. In top-down nanofabrication approaches, in order to obtain specific nanoscopic features, lithography techniques (physical top-down) or chemical processes (chemical top-down) are involved. NanoImprint Lithography (NIL) is a low cost top-down fabrication technique that implies the fabrication of micro and nanometer features by patterning onto polymeric films. Figure 1-3 illustrates one of the most simple fabrication approaches.

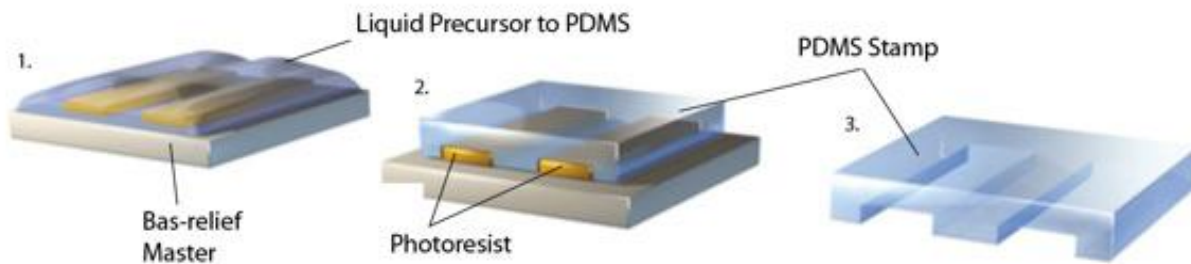


Figure 1-3: Fabrication process of a PDMS stamp. (Adapted from Whitesides & Love, 2001)

Bottom-up fabrication concept used for the fabrication of nanostructures exploits simple and small building blocks like atoms, molecules or nanoparticles that are self-assembled into larger and more complex structures. The majority of the bottom-up fabrication methods use chemically synthesized nanoparticles. One of the most common method used for the fabrication of solid substrates is the nanosphere lithography (NLS), based on the self-assembling of polystyrene or latex micro or nano-spheres on solid substrates followed by the deposition of a metallic thin film of desired thickness and subsequent removal of the spheres.

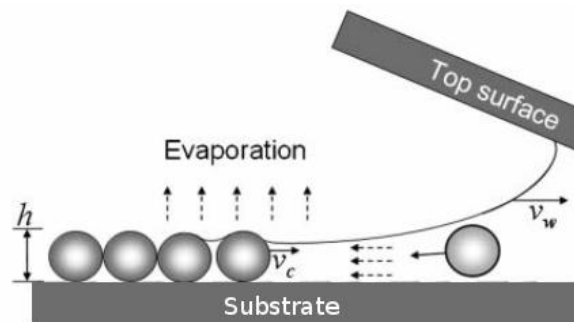


Figure 1-4: Schematic of the drying region of a thin evaporating film. The colloidal crystal of thickness h is deposited by translating the top surface with a speed v_w .

Nagayama et al. used a convective self assembling method, namely the *dip coating*, for fabricating a monolayer on a large area (Dimitrov and Nagayama, 1996; Rossi et al., 2000). During the convective assembly, the dispersed particles are brought together and crystallized in thin wetting films. A schematic representation is shown in Figure 1-4.

CHAPTER 2

FABRICATION OF NANOSTRUCTURED SUBSTRATES BASED ON GOLD NANOPARTICLES

In this chapter we address the following question: what types of Au NPs assemblies can be prepared by very simple methods, without using special equipment, to make SERS substrates of decent quality for SERS-based detection and analytical applications? Accordingly, we propose three different assembly strategies, which are very simple and easy to implement in any laboratory for the preparation of NPs films. The most simple relies on drop-coating, simply dispensing a drop on a substrate and allowing it to dry. The second method is based on chemically functionalized substrates, using molecular linkers to attach gold colloids on glass surfaces (Makiabadi et al., 2010; Toderas et al., 2007). The third technique is similar to drop casting method, but in this case a predefined shape is imposed on the colloidal drop by pinning the drop between a slide and the substrate, the setup being derived from convective self-assembly (CSA) (Bunzendahl et al., 2001; Ding et al., 2009; Prevo et al., 2005; Yuan et al., 2006); then NPs assemblies are obtained by drying.

The SERS activity of the resulting Au NPs assemblies is then investigated with respect to both signal intensity and reproducibility, by using a model Raman scatterer. Finally it is shown that the NPs assemblies prepared by chemical attachment and CSA are promising for use as SERS substrates for the detection and analysis of biologically relevant molecules, and also for the detection of multiple analytes in the same sample.

2.1 Fabrication of plasmonic substrate by assembling of gold nanoparticles

An important aspect in fabrication of plasmonic substrate by assembling of gold nanoparticles on solid substrate is to create a clean and hydrophilic surface on top of substrate. Depending of substrate types (e.g. microscope glass slide, polycarbonate plate or flexible polymers films) the cleaning and hydrophilization process is based on an ozone treatment.

In the following, we describe the three different assembly strategies proposed, which are very simple and easy to implement in any laboratory for the preparation of NPs.

2.1.1 Drop-casting method

The most usually employed method for fabrication of structures by assembling of micro and nanoparticles are the drop-casting method. A drop of colloid is placed onto a solid substrate.

The accumulation and deposition of colloids along the edge of the drop (meniscus, or triple-contact line) is induced by water evaporation that causes a flux of water containing colloids from the drop interior towards the meniscus. The colloidal drop remains pinned to the substrate during drying, the height of the drop decreases, and the dried deposit has almost the same footprint as the initial colloid drop, thus resulting in one circular strip. In our case, the Drop sample is prepared by simply dispensing a drop of Au colloid on the glass surface and allowing it to dry, a structure similar to so-called coffee-rings (Deegan et al., 1997) being obtained.

The drying process leads to the formation of a circular deposit, with a diameter of 6-7 mm, delimited by a thick edge 7-8 μm wide. The optical image of the dried colloidal drop is presented in Figure 2-1(a). As we can observe, the region delimited between dashed lines represents the coffee-ring. The arrow indicates direction from the drop edge to drop center.

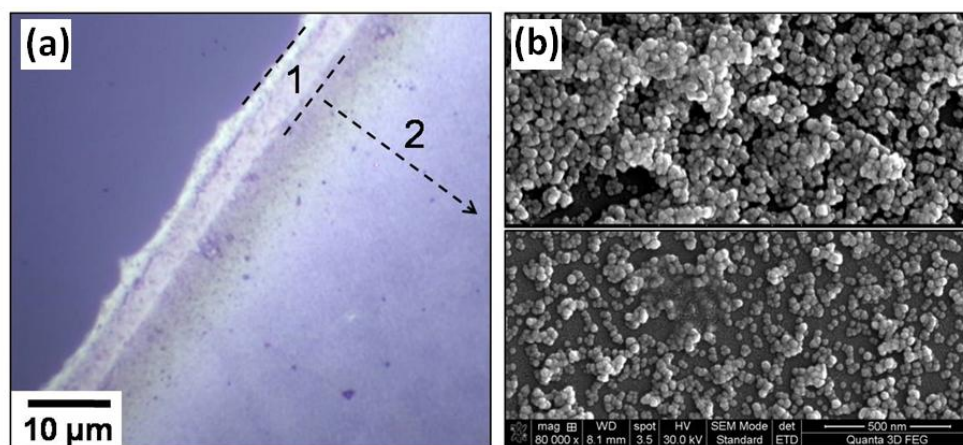


Figure 2-1: Optical microscopy (a) and SEM images (b) of NPs assemblies obtained by drying a colloidal suspension drop (Drop sample). Region 1 in (a), delimited by the dashed lines represents the so-called coffee-ring, while the arrow points toward the centre of the drop, indicating region 2.

2.1.2 Chemical attachment method

Another approach for fabrication of nanostructures based on assembled of nanoparticles is the chemical attachment of nanoparticles to a solid substrate by using a specific ligand between nanoparticles and solid substrate, such as aminopropyl trimethoxysilane (APTS) or mercaptopropyl trimethoxysilane (MPTMS). These molecules present on one side a silane group (SiH_4) for binding to glass slide (SiO_2) and on the other side an active amino ($-\text{NH}_2$) or mercapto ($-\text{SH}$) group that forms a strong covalent bond with gold nanoparticles (Baia et al., 2009). The morphology of sample, prepared by immersion of the functionalized glass slide into gold colloidal suspension appears as a rather uniform coating and is presented in the optical images (Figure 2-2(a)). Many Au NPs are individually attached to the substrate by formation of chemical bonds between gold nanoparticles and NH_2 groups of APTS. Many randomly deposited NPs aggregates, with a broad distribution of shapes and sizes can be also found on the Func sample, which correspond to the many bright spots in the optical image (Figure 2-2(a)).

Our suggestion is that a certain amount of APTS molecules are present on the glass slide surface which are not strongly bound to it and their detachment can induce the formation of these aggregates. Figure 2-2(b) gives an example of such a NPs aggregates with an irregular shape.

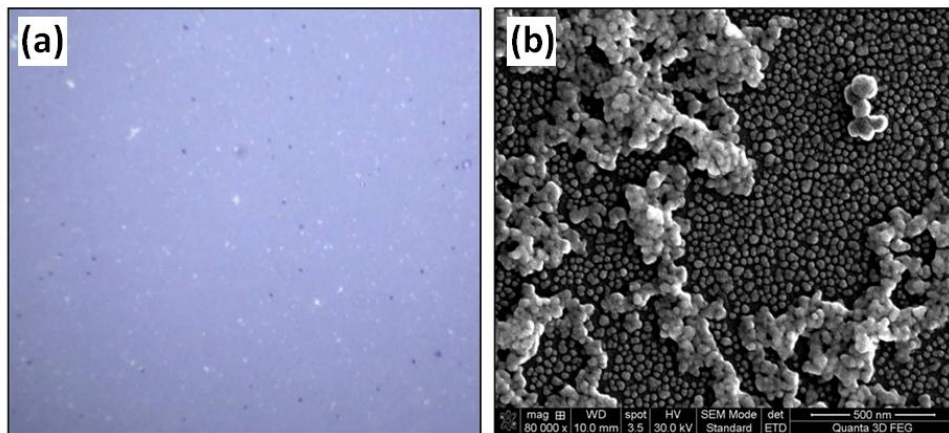


Figure 2-2: Optical microscopy (a) and SEM image (b) of NPs assemblies attached by chemical functionalization (Func sample).

2.1.3 Convective self-assembling method

For the third type of NPs assembly, a simple CSA setup was constructed, as follows: a rectangular glass slide is placed in loose contact with the glass substrate at an angle of 90° , with one edge parallel to the substrate. A colloid drop was dispensed along their contact area, and this drop was held in place by capillary forces, becoming thus elongated. In this way two straight menisci are formed on the substrate, one on each sides of the vertical plate. This trapped colloidal drop was allowed to dry in ambient conditions. Samples prepared according to this protocol are referred to as the CSA samples.

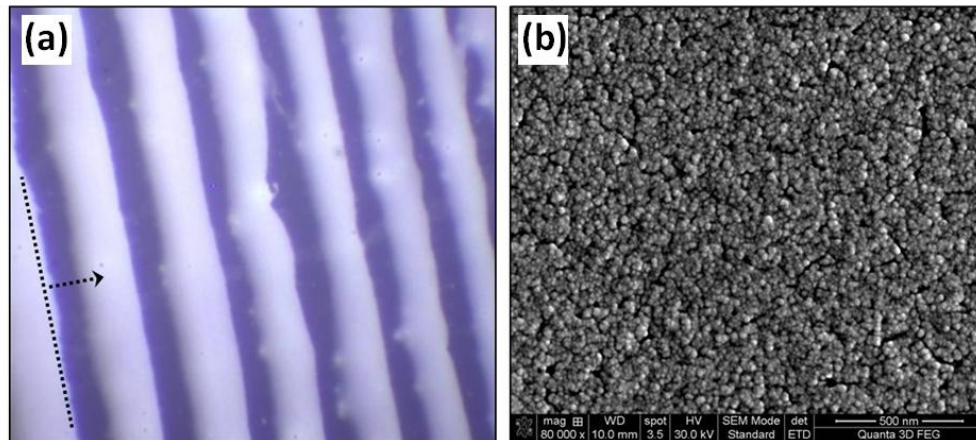


Figure 2-3: Optical microscopy (a) and SEM image (b) of NPs stripes prepared by convective assembly (CSA sample). The dotted line and arrow in (b) indicate the orientation and direction of translation of the meniscus during drying of the sample.

Therefore one obtains two triple-contact lines, which are now linear over 1-2 cm, one on each side of the vertical plate. The optical image in Figure 2-3(a) shows that a parallel array of strips, 6-10 μm wide, made of Au colloids was obtained upon drying on both sides of the vertical plate.

2.2 SERS performance of nanostructured substrates

The SERS response of the three types of NPs assemblies was tested for three different excitation laser lines. Figure 2-4 presents typical average SERS spectra recorded on each type of sample at each laser line. Spectra are collected from several points of a region (0.1×0.1 mm available through the piezo scan stage) and from several regions on the sample separated from each other by few millimeters.

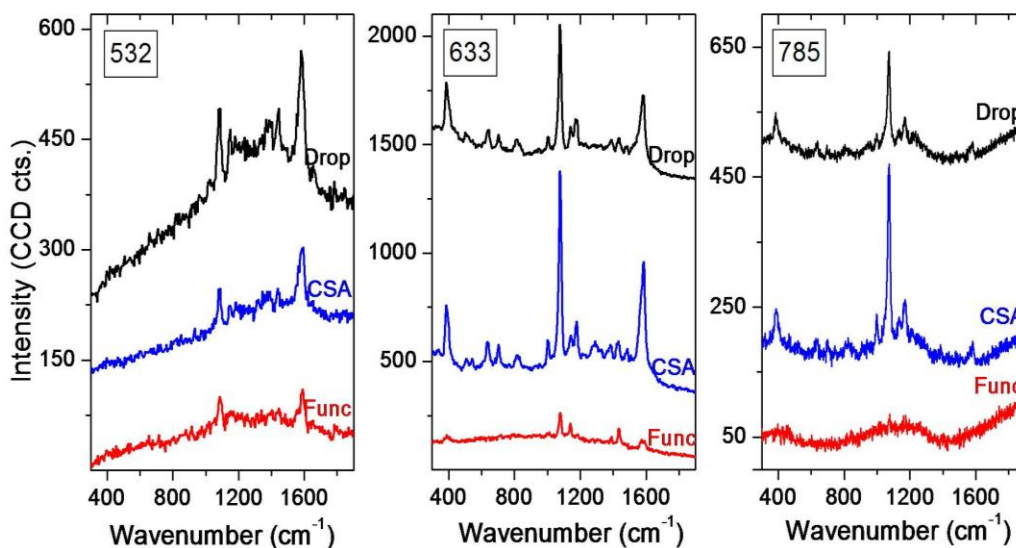


Figure 2-4: Average SERS spectra of p-ATP adsorbed on the three substrates, obtained at different laser excitations, as marked on the figure.

A first observation is that all types of samples are SERS active at the three laser lines, albeit they exhibit different efficiencies (Figure 2-4). An exception makes the Func sample which gives no signal at 785 nm, in the used experimental conditions. At 532 nm all types of assemblies yield a modest enhancement, with Drop having the most intense averaged spectrum, then the CSA sample, while the Func sample exhibits the weakest intensity. The spectra recorded at 633 nm are the best quality ones, in terms of signal to noise ratio, and in terms of their spectral richness. SERS bands at 388, 637, 705, 1178 cm^{-1} (and others less intense) are also clearly distinguishable, beside the most intense bands at 1079 and 1584 cm^{-1} . The order of spectrum intensity, starting from the most intense, is in this case CSA, Drop, Func. At 785 nm excitation good spectra are again obtained, with CSA yielding higher bands intensities than Drop, and no signal for Func, as already mentioned.

As these results point out, 633 nm is the most efficient excitation wavelength, providing high signal to noise ratio, a rich spectral signature, at low excitation powers. We further discuss the uniformity of each type of substrate in terms of spectrum shape and intensity across the sample surface. Figure 2-5 presents collections of SERS spectra recorded at different spots on each sample under 633 nm excitation.

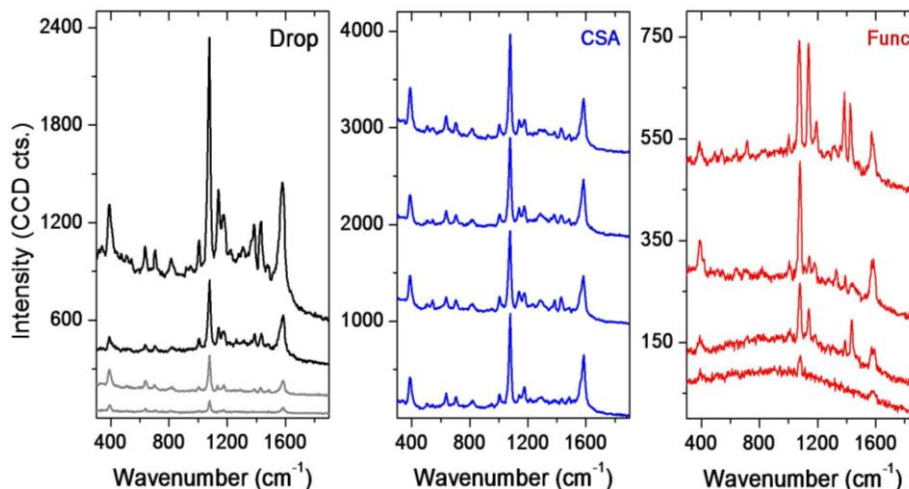


Figure 2-5: Several SERS spectra of p-ATP recorded at different sites on each of the three types of substrates at 633 nm laser excitation.

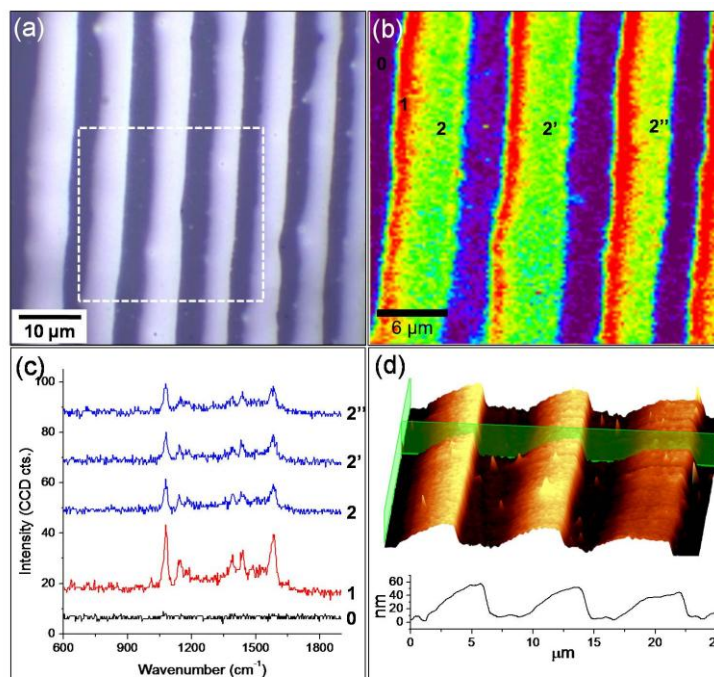


Figure 2-6. SERS imaging on NPs strips obtained by CSA: (a) optical microscope image; (b) image obtained by plotting the intensity of the p-ATP SERS spectra across the area marked by the rectangle in (a); (c) SERS spectra at the sites marked in panel (b); (d) AFM image of NPs strips obtained by CSA.

For the Drop, very large variations can be observed ($\pm 90\%$) from the thick solid circular edge to the central part of the deposit. The strips on the CSA sample exhibit a highly uniform signal, the presented spectra being recorded on different strips, with the collection point being selected midway between the strip's edges. Variation of the 1080 cm^{-1} band intensity lies within a considerably narrower $\pm 13\%$ range. The Func sample presents again strong spot-to-spot variations both in spectral shape and SERS band intensity ($\pm 70\%$).

To further investigate this uniformity SERS imaging was performed. The rectangle in Figure 2-6 (a) marks a region on the CSA sample that was scanned with a confocal microscope in Raman imaging mode. The signal intensity appears very homogenous on the strips' surface, except the left edges of the strips, where the intensity is higher. To understand the 'edge' effect, AFM was performed on the NPs strips, and a typical result is presented in Figure 2-6d.

As observed in the AFM cross-section the NPs strips are thinner on one side. This shape asymmetry was already observed previously (Farcau et al., 2010; Lee et al., 2009) on NPs assemblies obtained by CSA, and is related to the meniscus shape and its direction of translation during the stick-slip deposition process. Thus, the obtained results point out that the thinner side of the NPs strips, which is a monolayer of NPs, provides a higher enhancement than the rest of the strip, where the NPs assembly adopts a thick multilayer morphology

2.3 Application of plasmonic substrates in multi-analyte detection of biomolecules from biological fluids

2.3.1 Multi-analyte detection

The CSA substrate was first immersed overnight in 10^{-5} M ethanol solution of cytosine. Then the substrate was washed with ethanol and immersed in 10^{-4} M methanol solution of p-ATP for 1 hour. As shown in Figure 2-7, high quality SERS spectra were recorded under 633 nm laser excitation after exposure of the NPs strips to the 10^{-5} M solution of cytosine (spectrum i).

The illustrated spectrum clearly identifies the presence of cytosine molecules on the CSA sample. The two strong bands at 805 and 1640 cm^{-1} are assigned to breathing vibration of the whole molecule and to the combination of C5-C6 stretching mode and NH_2 scissoring, respectively (Sánchez-Cortés and García-Ramos, 2001). The band at 1194 cm^{-1} arises from N1-C2, C2-N3 stretching vibrations (Sánchez-Cortés and García-Ramos, 2001). The bands at 1324 and 1438 cm^{-1} are attributed to in-plane bending of all H atoms and to stretching vibrations of N1-C6, N3-C4, respectively. The band at 1597 cm^{-1} corresponds to the combination of C5-C6 stretching vibration and NH_2 scissoring.

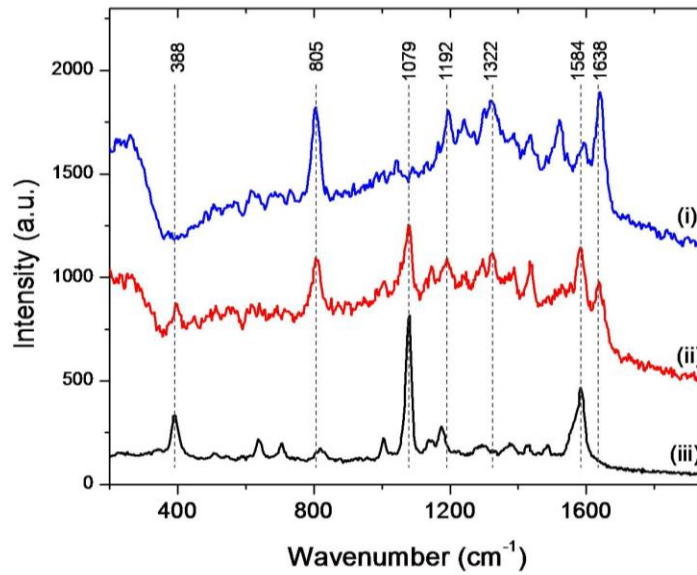


Figure 2-7. SERS spectra obtained on CSA samples by exposure to: (i) 10^{-5} M cytosine; (ii) 10^{-5} M cytosine followed by 10^{-4} M p-ATP; (iii) 10^{-4} M p-ATP. The spectra were recorded using a 633 nm laser excitation line.

2.3.2 Detection of urea trace in biological fluids

Figure 2-8 presents the SERS spectra of tear, fingerprint, urine and urea, deposited on the gold colloids particulate film, together with the normal Raman spectra of solid urea and the scattering signal of the particulate film.

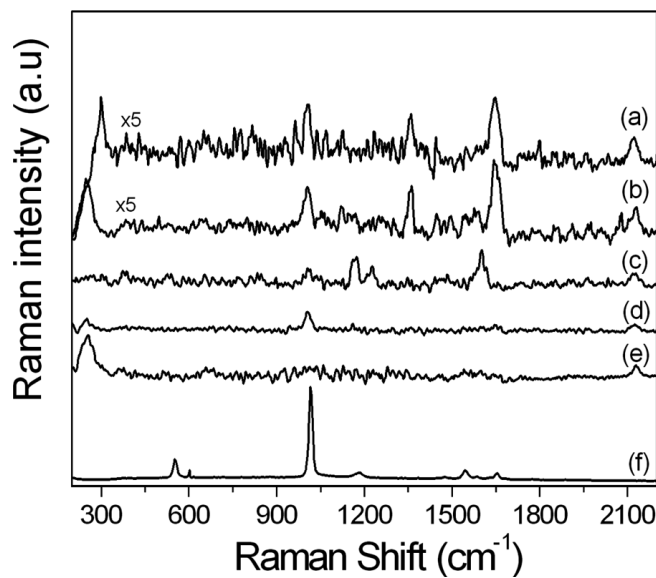


Figure 2-8: SERS spectra of (a) tear, (b) fingerprint, (c) urine and (d) urea, together with the reference Raman spectra of (e) the substrate and (f) urea.

Urea ((NH₂)₂CO) is a simple organic molecule which has two amino groups (–NH₂), bound by a carbonyl group (–C=O). Keuleers et. al. reported an extensive study on the vibrational analysis of urea (Keuleers et al., 1999). The recorded Raman spectrum of urea is dominated by the symmetric N–C–N bond stretching vibration at 1016 cm⁻¹ (see Figure 2-8, spectrum f), which was subsequently used for the analysis of urea. The detection of lower-level amounts of urea in body fluids requires the use of SERS technique.

CHAPTER 3

FABRICATION OF MICROPATTERNED NANOSTRUCTURED SUBSTRATE FOR MULTIPLICATIVE ELECTROMAGNETIC SERS ENHANCEMENT

In this chapter we present a self-assembly approach for the fabrication of highly active dual-scale SERS substrates based on colloidal gold nanoparticles. By employing Convective Self-Assembly (CSA) of a colloidal mixture of 15 nm gold nanoparticles (AuNPs) and 500 nm polystyrene microspheres (PsMSs), followed by solvent removal of the polymer, a periodically micro-patterned film made of colloidal gold nanoparticles is obtained.

We evidence a multiplicative SERS enhancement, by analyzing the SERS response in comparison with a planar non-patterned AuNP film, and discuss the results in correlation with optical reflectivity spectra and FDTD simulations. We also explore spot-to-spot reproducibility and time stability of the fabricated dual-scale colloidal SERS substrates.

3.1. Fabrication of periodically micro-structured gold nanoparticle films

A colloidal mixture of spherical gold nanoparticles (AuNPs) with a concentration of 13×10^{13} particles/mL and polystyrene microspheres (PsMS), 2% w/v in aqueous suspension, was prepared in a volume ratio of 1/100 PsMS/AuNPs.

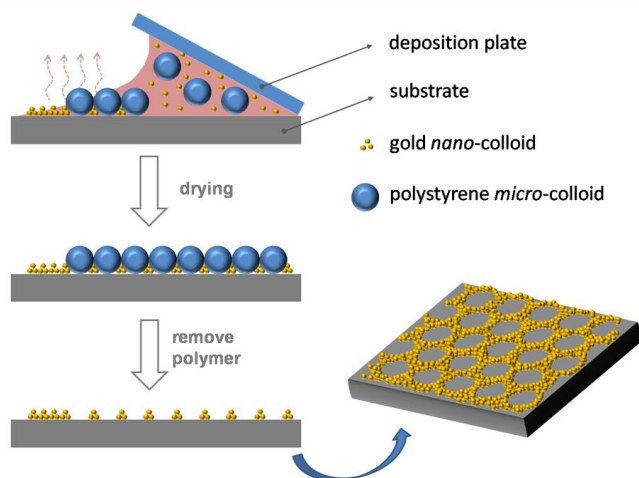


Figure 3-1: Fabrication process of Au NPs micro-structured film by BiCSA. Water is evaporated in a constrained geometry from a mixed colloidal suspension of AuNPs and PsMS. After drying, the PsMS are dissolved in chloroform.

A clean glass slide (deposition plate) was placed in oblique position (at an angle of about 15°) with respect to the horizontal glass slide. A drop ($5 \mu\text{l}$) of colloidal mixture was inserted in the V-shaped groove formed by the substrate and deposition plate, along their contact area, see Figure 3-1. The drop is held by capillary forces, and a straight meniscus is thus formed on the substrate. Then water is evaporated in ambient laboratory conditions. It is expected that the Au nano-colloids will assemble into the interstices available within the ordered array of polymer micro-colloids. The last step was to dissolve the PsMS by immersing the substrate in chloroform for 30 minutes.

3.2 Characterization of periodically micro-structured gold nanoparticle films

3.2.1 Morphological characterization

SEM images (Figure 3-2 a, b), an ordered hexagonal lattice of bowl-shaped apertures was obtained after dissolving the PsMSs. The obtained two-dimensional pattern is consistent with the typical hexagonal pattern obtained by CSA of spherical colloids, i.e. polystyrene, PMMA, or silica microspheres. For simplicity, we shall call it AuNP micro-structured film, shortly AuNP μ -Struc film from here on. Note the close resemblance of the morphology of this films with that of the spherical void arrays developed in Baumberg's group (Cole et al., 2007; Kelf et al., 2006).

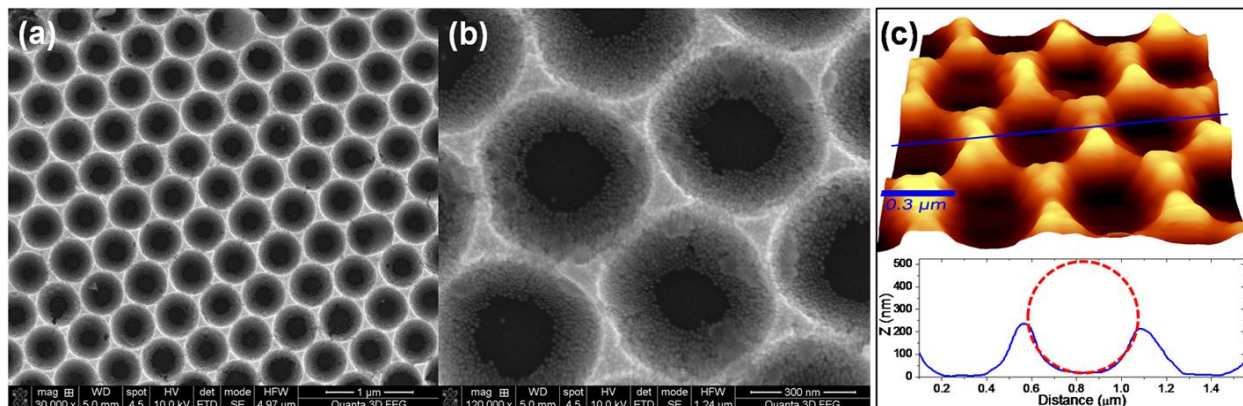


Figure 3-2: (a,b) SEM images of AuNP μ -Struc film; (c) AFM image of AuNP μ -Struc film (top), and cross-section along the indicated line (bottom); the dotted line is part of a circle with 500 nm diameter, suggesting the position of a Ps microsphere prior to its removal..

In Figure 3-2 b, a zoom-in SEM image of the AuNP μ -Struc film reveals that the constituent Au colloids were assembled in a highly compact manner.

3.2.2 Optical characterization

The reflectivity spectra are presented in Figure 3-3. The μ -Struc AuNP film presents a more structured spectrum, with several minima and maxima in the region between 550 and 900

nm. On both types of samples the reflectivity is low around 500 nm, due to interband transitions in gold. The modulations in the spectrum of the μ -Struc film are induced by the periodic pattern, and are attributable to resonant light scattering by the periodic lattice. We suggest that a Bloch-type propagating mode of photonic (as opposed to plasmonic) nature is observed.

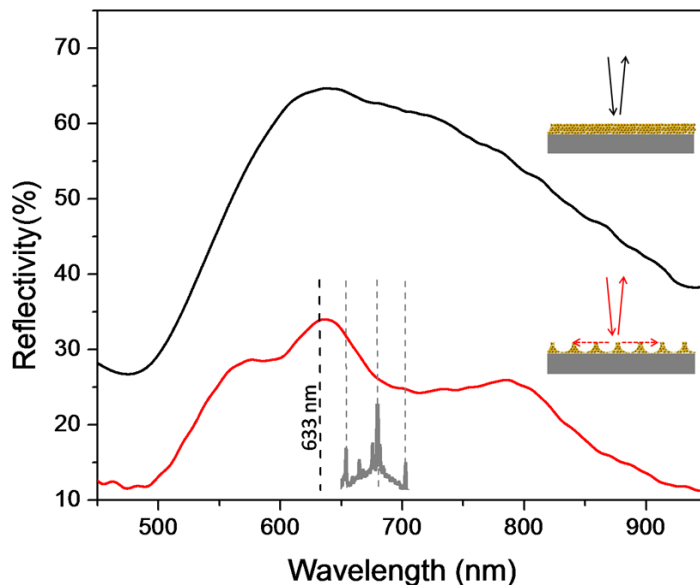


Figure 3-3: Reflectivity spectra of AuNP μ -Struc film (bottom) and AuNP Flat film (top). The 633 nm laser line and the region corresponding to the interval $500\text{cm}^{-1} - 1600\text{cm}^{-1}$ in the associated Raman spectrum are marked.

3.3 Assessment of multiscale electromagnetic SERS enhancement

3.3.1 SERS performance

In the following we were interested to investigate if a supplementary Raman enhancement arises from such morphological configuration. Considering this, the first assessment of the SERS activity of the AuNP μ -Struc films was conducted using BSPP as an ‘internal’ Raman probe. Three different excitation laser lines (532 nm, 633 nm and 785 nm) were used to perform the experiments. Comparative experiments between the two distinct sample regions (μ -Struc film and Flat film) were carefully conducted to evaluate their SERS response. Characteristic bands of BSPP molecules were observed for all three excitation lasers, from both μ -Struc film and Flat film as can be seen in Figure 3-4. An important observation is that in each case, the μ -Struc film gives a SERS signal of larger intensity than the Flat film. The SERS intensities were evaluated by integrating the BSPP SERS band at 1084cm^{-1} . From the integrated values we conclude that a multiplicative enhancement of SERS signal is present on the μ -Struc film as compared with the Flat film. In order to confirm this effect it should be first verified if the source of supplementary signal enhancement can be attributed to differences in the active gold

surface. The calculated ratio between the exposed areas is of approximately 1.6 in favour of the μ -Struc film. Although it is difficult to have a very precise measure of the active surface, this rough estimate is far from a factor 5, the larger value obtained for the SERS band intensity ratio.

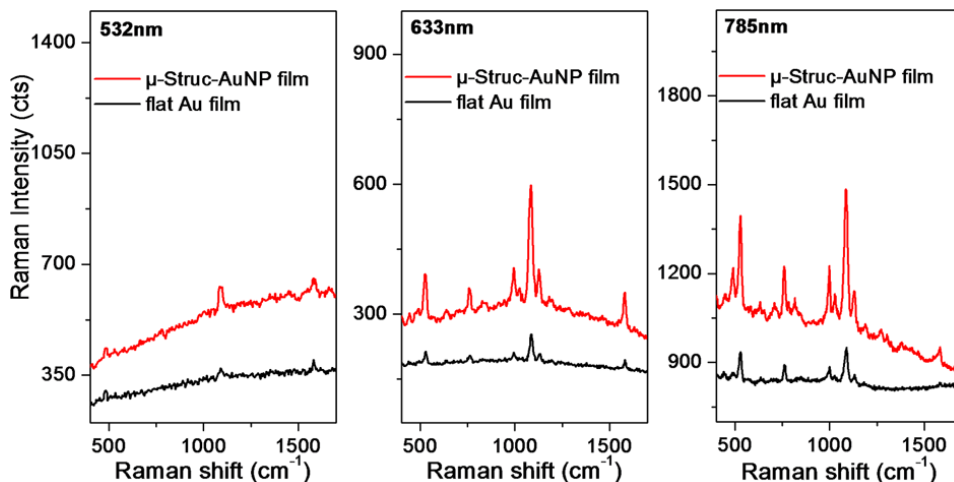


Figure 3-4: SERS spectra from BSPP-capped AuNP μ -Struc film (top spectra) and Flat film (bottom spectra), obtained at different laser excitations, as marked in the panels.

Furthermore we explore the SERS efficiency of the fabricated substrate by using another Raman reporter, cresyl violet (CV), which was deposited on the NPs films after their fabrication, therefore is expected to be adsorbed mostly at the films' surfaces. Figure 3-5 illustrates the SERS spectra of CV under three laser excitations, again comparing responses from μ -Struc film with those from Flat film samples.

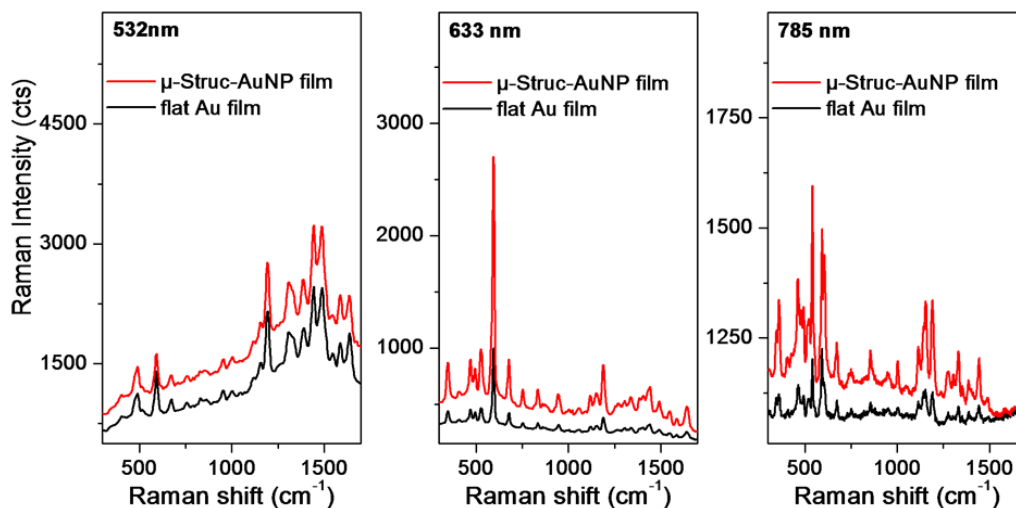


Figure 3-5: SERS spectra of Cresyl violet molecules adsorbed on AuNPs μ -Struc film (top spectra) and Flat film (bottom spectra), obtained at different laser excitations, as marked in the panels.

The intensity of the CV SERS band at 594 cm^{-1} (assigned to NH_2 rocking (Vogel et al., 2000)), was selected to quantify the difference in the SERS intensity between spectra collected from μ -Struc film and Flat film. Again, a net supplementary enhancement effect is observed under 633 and 785 nm excitations. No net intensity differences between the two types of surfaces were observed when 532 nm excitation was applied.

3.3.2 Spot to spot reproducibly, time stability and reutilization

Beside a good enhancement, the reproducibility and stability of the SERS signal are important issues to be addressed in order to consider a SERS substrate reliable. To demonstrate the SERS reproducibility of the prepared periodically patterned AuNPs film, SERS spectra of CV analyte were recorded from random multiple sites on the substrate surface, under 633 nm excitation. Figure 3-6 a presents a colormap of 15 such spectra.

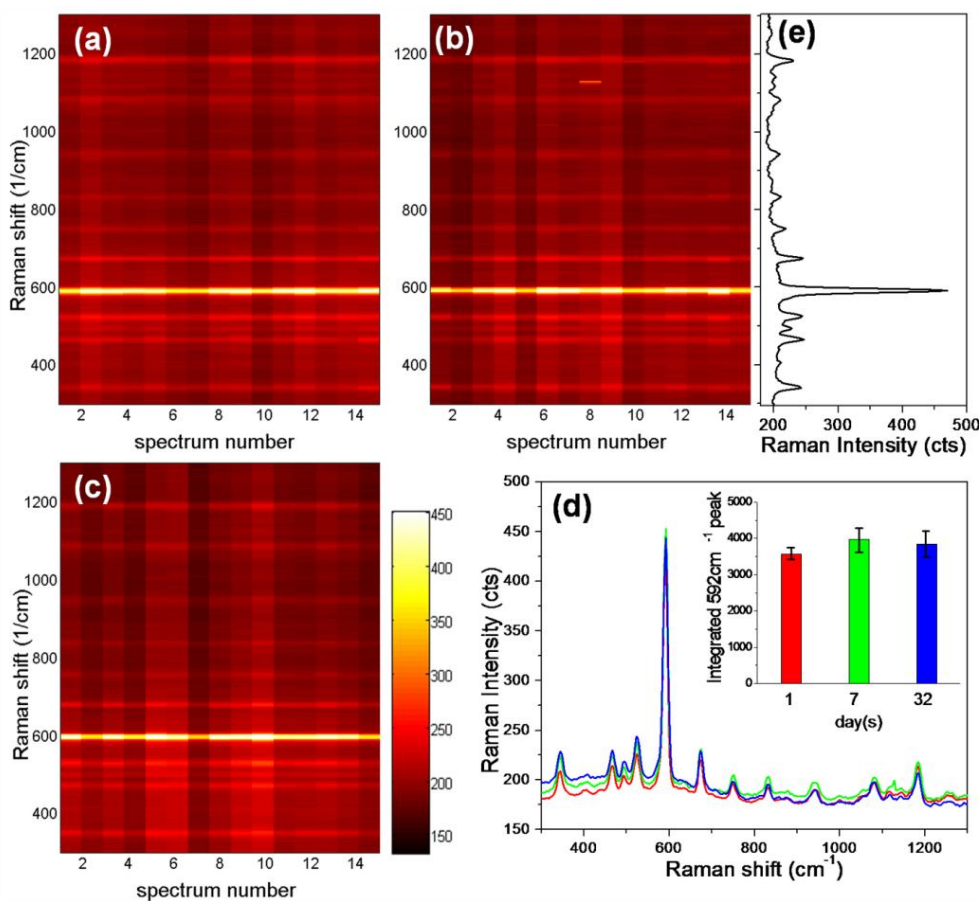


Figure 3-6: (a-c) Colormap representation of several SERS spectra collected at different sample sites at different time: (a) t_0 ; (b) $t_0 + 7$ days; (c) $t_0 + 30$ days. (d) Average SERS spectra corresponding to the colormaps in (a-c); inset represents the intensity of the 594 cm^{-1} SERS band and the standard deviation. (e) A typical SERS spectrum, for helping colormap visualization.

We observe that the intensity and spectral position of the SERS bands is relatively constant, indicating a good homogeneity of the sample. To test the time stability of the signal we performed a similar analysis after 7 (Figure 3-6 b) and 30 days (Figure 3-6 c). As Figure 3-6 a-c demonstrates, the features of the SERS spectra are stable, hence the fabricated substrate shows good stability and reproducibility over time.

3.3.3 Finite differences time domain (FDTD) simulations

Two-dimensional FDTD simulations were performed, which, although not able to quantitatively reproduce experimental results with high accuracy, can provide sufficient qualitative, phenomenological information.

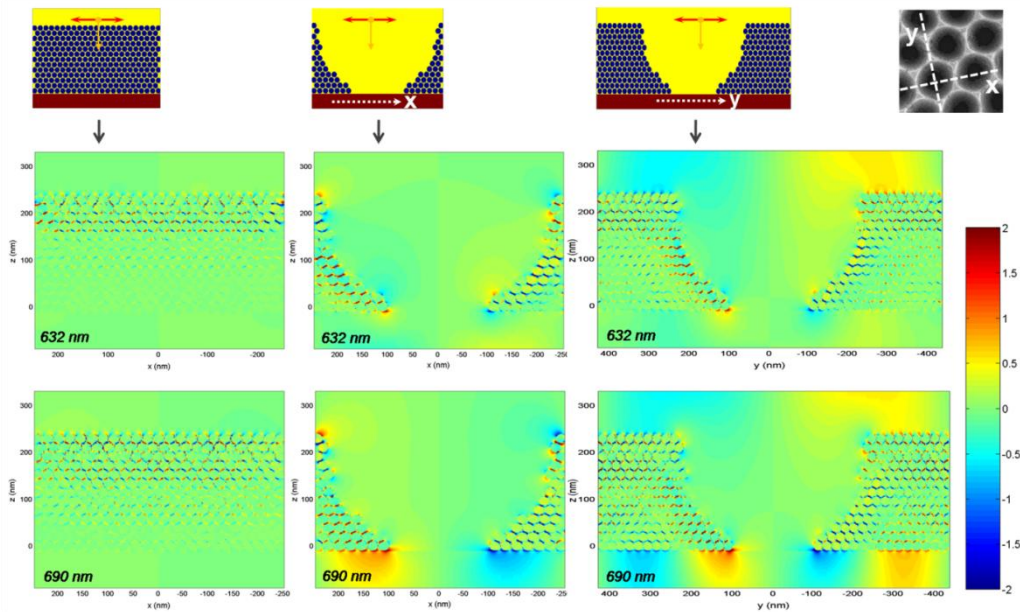


Figure 3-7: Schemes of the simulated configurations, with axes, electric field polarization and propagation direction of incident light indicated (top row). E_z component of the electric field at 632 nm, corresponding to the excitation wavelength (middle row). E_z component of the electric field at 690 nm, corresponding to Raman-scattered photons.

As can be observed on Figure 3-7, for the Flat NPs film, an E_z component can be found only in the gaps between nanoparticles. Also, one can note that light penetrates only the first 3-4 NPs layers, and that this penetration depth is slightly larger for the larger wavelength. When analyzing the μ -Struc film, some additional electric field can be observed, both above the film and below, in the substrate, at both 632 nm and 690 nm.

CHAPTER 4

FABRICATION OF ORDERED PLASMONIC SUBSTRATE FOR DETECTION AND QUANTITATIVE ANALYSIS USING SERS

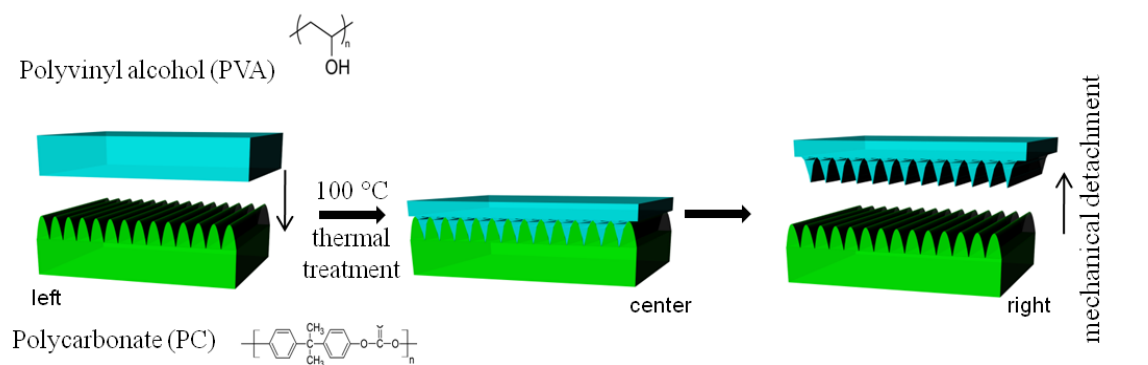
In this chapter we present a simple approach for the fabrication of periodically ordered pyramidal-shaped metallic nanostructures using a low-cost method which does not involve a complex fabrication process. This approach is based on the nanoimprint lithography (NIL) and exploits the thermal properties of two classes of polymers, thermoplastics and hydrogels. In this study, we used polycarbonate (PC) as thermoplastic polymer and polyvinyl alcohol (PVA) as hydrogel polymer because it is easily soluble in water, exhibits excellent chemical resistance and physical properties, but also presents good mechanical properties in dry state (Park et al., 2001). Knowing the thermal properties of these polymers, we manage to texture the PC with PVA using NIL and a commercial Digital Versatile Disc (DVD) as initial mold in a two imprinting steps process. This technique represents a low-cost alternative to the classical lithography techniques, allowing the fabrication in a controlled and reproducible manner of periodic highly ordered nanostructures over large areas ($\sim\text{cm}^2$).

Furthermore we were interested in exploiting the pyramidal-shaped nanostructured substrate for the detection and quantitative analysis with high sensitivity of relevant biomolecules (e.g. urea) as this approach offers the possibility to develop novel biosensors capable to detect relevant biomolecules at extremely low concentrations.

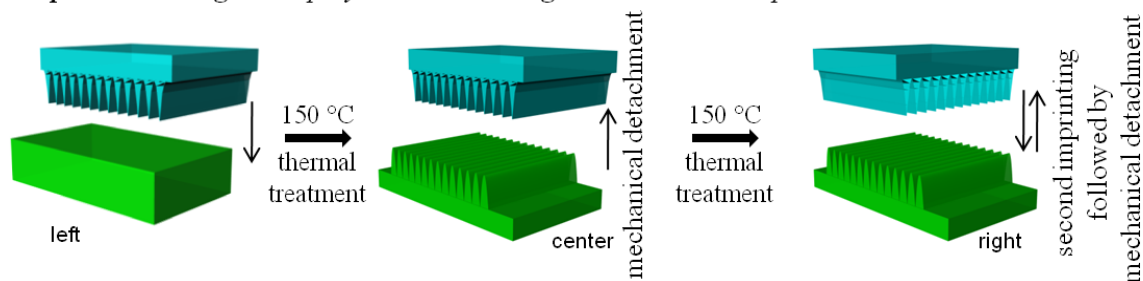
4.1 Two step fabrication process of pyramidal shaped substrate through nanoimprinting lithography

In order to prepare the pyramidal-shaped substrate, a thin film of PVA was first deposited over the clean polycarbonate side using an aqueous solution of 20 wt% PVA, (see Scheme 4-1, step1, left). After a subsequent thermal treatment at 100°C for 20 minutes (see Scheme 4-1, step1, center), the PVA film was mechanically detached from the surface of the polycarbonate platform. As we expected, the detached PVA film presents, after transfer, the same structural characteristics as the DVD surface (see Scheme 4-1, step 1, right). This textured PVA film was subsequently used as mold for stamping the PC surface of the DVD. Therefore, the second step consisted in placing the DVD polycarbonate and the textured PVA stamp between two microscope glass slides, (scheme 4-1, step 2, left). A constant force was applied from both sides followed by a thermal treatment at 150°C for 15 minutes, (see Scheme 4-1 step 2, center). Knowing that the DVD polycarbonate is a thermoplastic that easily melts during the heating process (Neil et al., 2007), the polycarbonate surface was thus imprinted with the structural characteristics of the DVD (see Scheme 4-1, step 2, center). The final step consisted in detaching the PVA stamp and quickly rotating it with 90°C and performing a second imprinting of the thermoplastic polymer following the above described procedure (see Scheme 1, step 2, right).

Step 1 : Creating a PVA mold using a DVD polycarbonate template



Step 2 : Texturing DVD polycarbonate using PVA mold as template



Scheme 4-1: Two-step process of fabrication of pyramidal-shaped substrate. Step one represents the transfer of the mold characteristics to the hydrogel film, the second step represent the imprinting of hydrogel film characteristics to thermoplastic film at different angle.

4.2 Characterization of pyramidal-shaped plasmonic substrate

4.2.1 Morphological characterization

A characteristic AFM image of the commercial DVD polycarbonate is presented in Figure 4-1 a along with an AFM image of the resulting textured PVA film. The analysis of the AFM image of the DVD reveals a groove like structure with a height of 100 nm and width of 723 nm, see Figure 4-1 a.

After being imprinted with the groove like structure of the DVD polycarbonate mold, the PVA film displays a morphology very similar to the original DVD (see Figure 4-1 b). The PVA film present a height of around 65 nm, this differences in height observed being given by the melting of the DVD polycarbonate during the thermal treatment.

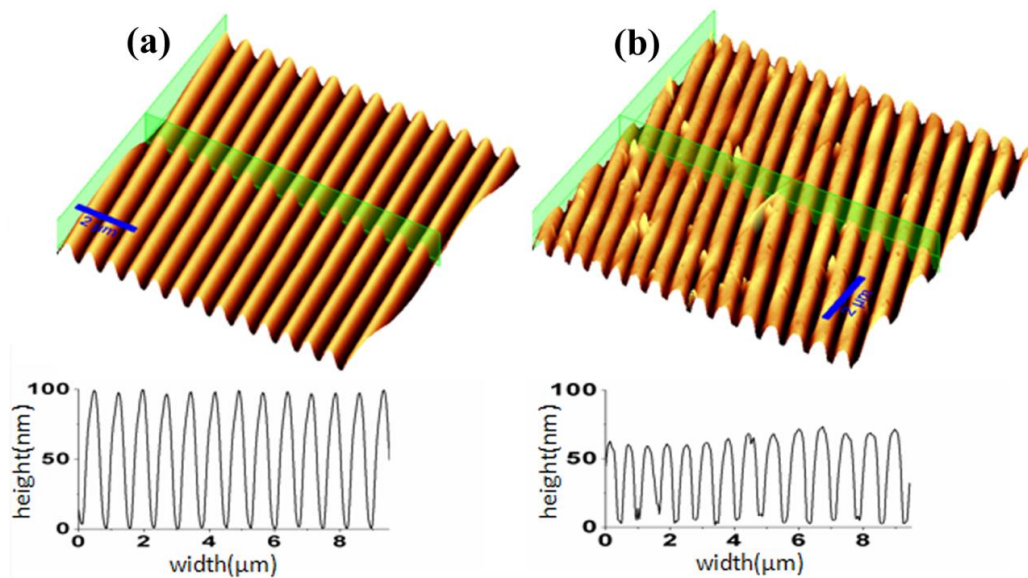


Figure 4-1: AFM images of commercial DVD (a) and textured PVA film (b). Cross section of each AFM image represents the height and the width of the structures. Scale bars: 2 μm .

In Figure 4-2 we present the 3D AFM image of pyramidal-shaped nanostructure along with crosssections over two directions.

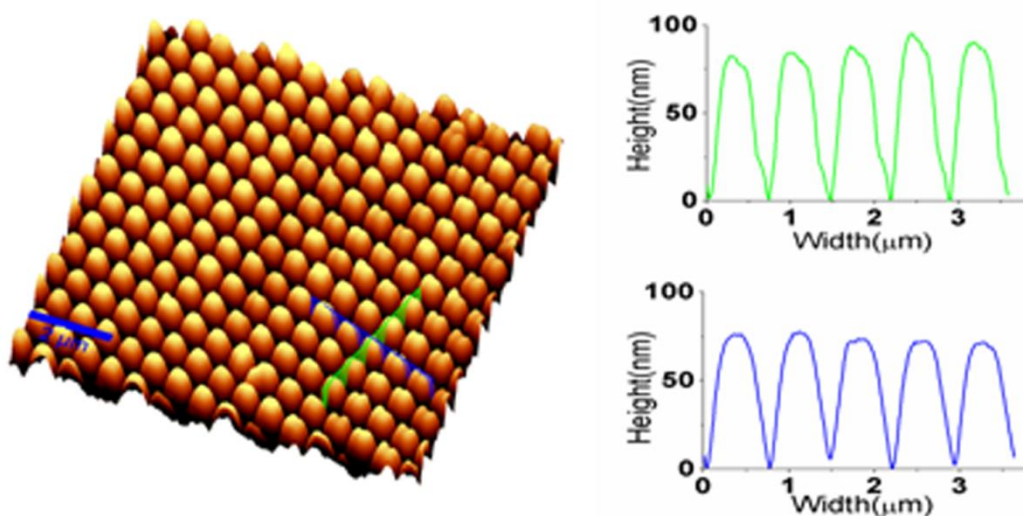


Figure 4-2: 3D AFM image of pyramidal-shaped substrate and two cross sections representing the directions of imprinting. Scale bar: 2 μm .

This slightly difference can be considered as a consequence of the different times used for the thermal treatments performed during the two steps of imprinting, of 15 and 10 minutes, respectively.

4.2.2 Optical characterization

Figure 4-3 presents the normal incidence transmission and reflectivity spectra of the fabricated structure. The recorded transmission spectrum exhibits two distinct maxima at 741 and 815 nm, respectively, which are well reproduced by the two distinct minima in the reflectivity spectra.

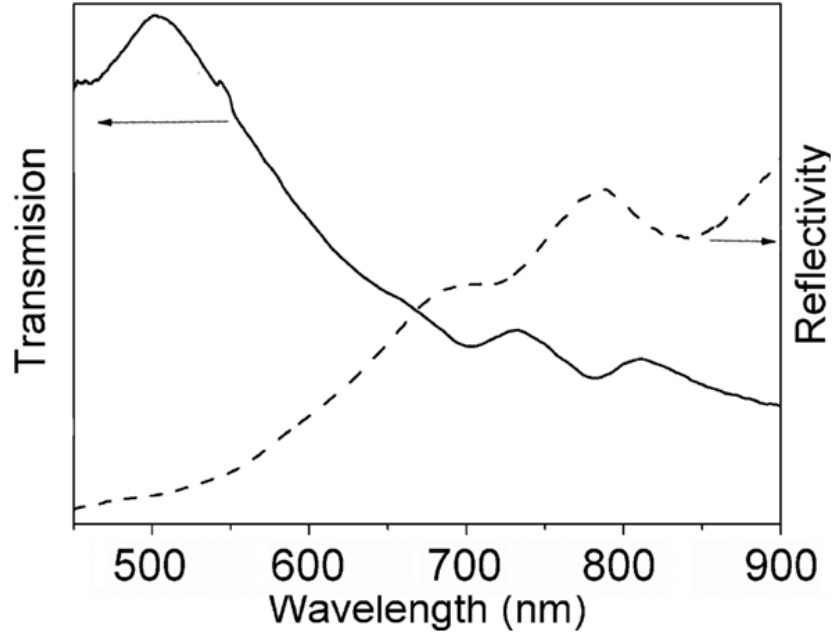


Figure 4-3: Transmission (solid line) together with reflectivity (dash line) spectra on gold-coated pyramidal-shaped substrate.

A better understanding of the origin of these two bands was attained from transmission measurements conducted at various incident angles between 0 and 30°. Both transmission maxima were found to exhibit a progressive blue-shift with increasing light incidence angle. This behavior suggests that they originate from the excitation of propagative surface plasmons by a grating coupled mechanism. Knowing that the fabrication process consists of a two-step imprinting procedure, we can assume that the size of the pyramids and the period between them are slightly different over the two directions. We can therefore infer that two minima correspond to propagative surface plasmons along the two directions of the pyramidal-shaped structure.

4.2.3 Finite differences time domain (FDTD) simulations

In order to get a better insight into the experimental optical response of the fabricated structure, we conducted numerical simulations by employing the FDTD. The reflectivity spectra obtained for this structure and the two possible polarizations are presented in Figure 4-4. From the simulated spectra we observe that there is a correlation between the position of the reflection minimum and the period of the array over the two directions. Therefore, the origin of the two

optical bands can be assigned to propagative surface plasmons over the y and z axis of the structure.

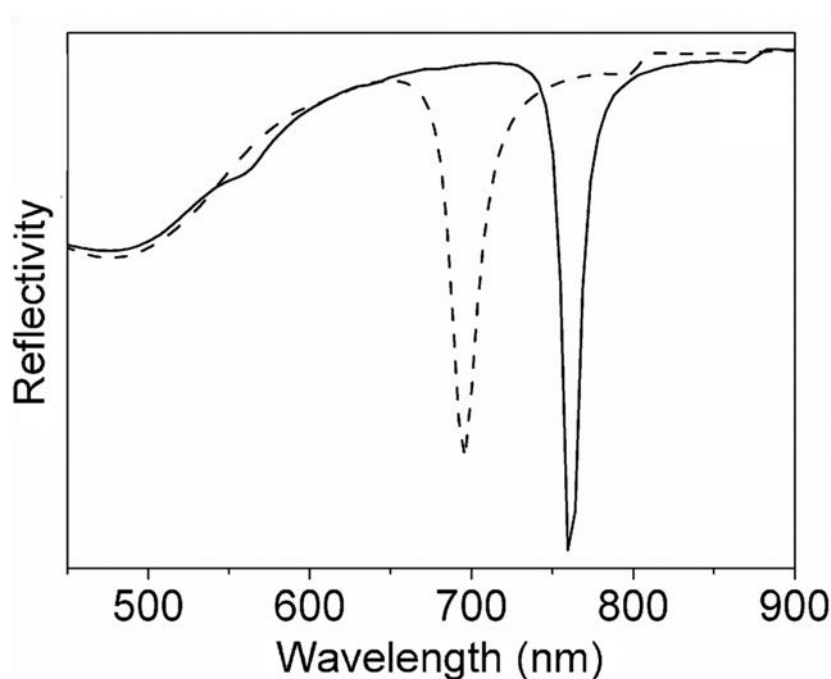


Figure 4-4: FDTD-simulated optical reflectivity spectrum of pyramidal-shaped substrate obtained at normal incidence by using a source with polarization parallel to the y axis (solid line) and z axis (dash line).

4.3 Spectroscopic properties of pyramidal-shaped plasmonic substrate

We have chosen to test the SERS response of the pyramidal-shaped substrate under excitation with the 785 nm laser line in order to excite the plasmonic band showed in the reflectivity spectrum. Figure 4-5 presents the SERS spectrum of p-ATP molecule adsorbed onto the fabricated plasmonic substrate through incubation of the substrate into a 10^{-4} M methanol solution of p-ATP for 24 hours, together with the reference Raman spectrum of p-ATP in powder state.

Compared to the normal Raman, in the SERS spectrum of p-ATP, the C-S stretching vibration is shifted to 1076 cm^{-1} due to the covalent bonding of the molecules to the gold substrate (Baia et al., 2009). In addition, we observe a moderate increase in intensity of the peak from 1178 cm^{-1} as well as the emergence of two new bands around 1141 and 1386 cm^{-1} .

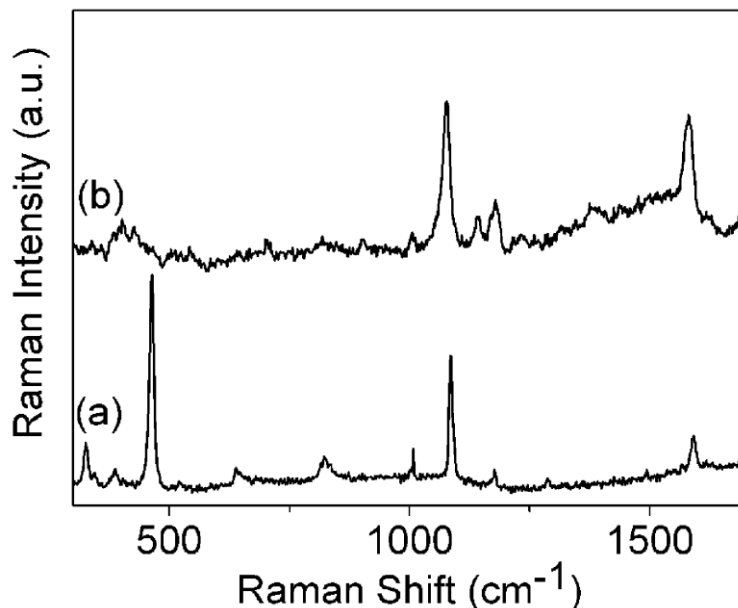


Figure 4-5: (a) Raman spectrum of p-ATP in powder state and (b) SERS spectrum of p-ATP adsorbed on the pyramidal-shaped substrate.

4.4 Detection and quantitative analysis of urea molecules

In order to test the applicability of the fabricated substrate for biological applications we studied the efficiency of the pyramidal-shaped structures in detecting the adsorption of a relevant biomolecule. For this purpose we choose urea which is an important biomarker for different renal diseases. Urea is a simple organic molecule, containing one carbonyl group, ($>C=O$) and two amino groups ($-NH_2$).

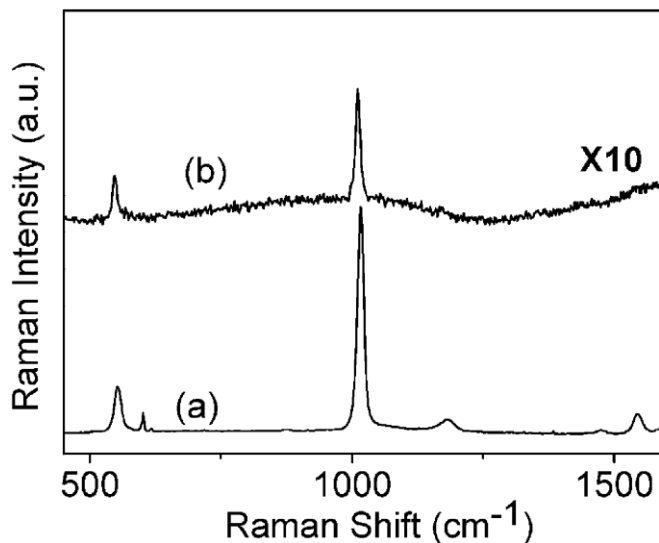


Figure 4-6: (a) Raman spectrum of urea in powder state and (b) SERS spectrum of urea molecule adsorbed on the pyramidal-shaped substrates.

As shown in Figure 4-6, the Raman spectrum of urea in powder state (spectrum (a)) presents four dominant vibrational peaks located at 552, 1016, 1181 and 1545 cm^{-1} , which, according to previous literature reports, can be assigned to N-C-O bending, symmetrical C-N stretching, NH_2 rocking and NH_2 bending vibrations (Keuleers et al., 1999)

The presence of urea dominant C-N stretching mode at 1010 cm^{-1} in the spectrum of urea recorded after the adsorption of the molecules onto the pyramidal-shaped substrate, along with the absence of NH_2 specific vibrational modes from the spectrum, demonstrate the successful SERS detection of urea molecules in low concentration.

Furthermore, due to the periodicity of the pyramidal-shaped structure, the fabricated substrate can be exploited not only for the detection of the adsorption of the urea molecules but also for the correlation of the concentration of urea with the Raman intensity of the dominating band of urea.

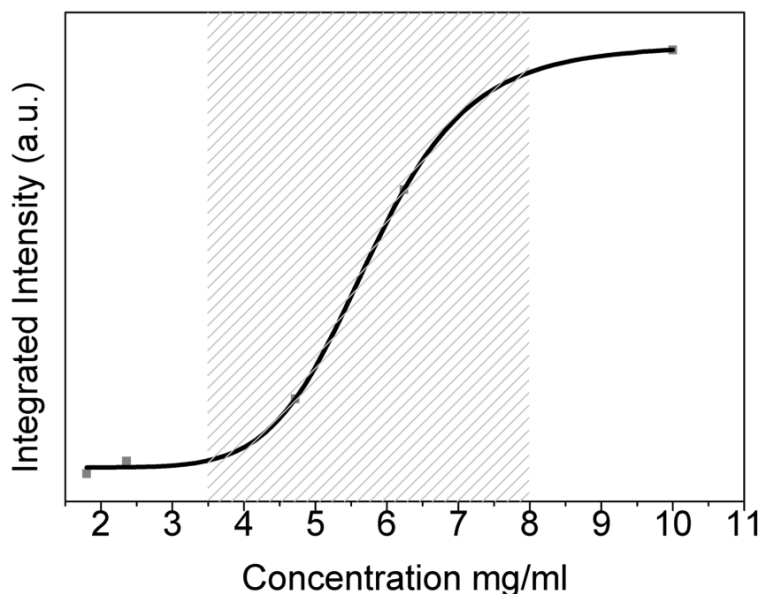


Figure 4-7: Concentration dependence of the integrated intensity of the N-C-N characteristic band of urea. The marked area outlines the concentration range with the maximum efficiency of the fabricated structures.

Figure 4-7 shows the obtained calibration plot, correlating the concentration of urea with the corresponding intensity of the N-C-N characteristic SERS band.

The obtained calibration plot demonstrates that the fabricated plasmonic substrate can be efficiently employed for the detection of urea in the 3.5 – 8 mg/ml concentration range. Therefore, we can claim that using our pyramidal-shaped substrate it is possible to realize a biosensor capable to determinate the pathological state of kidneys by making quantitative analysis of urea using SERS and alternative biological fluids.

CHAPTER 5

FINAL CONCLUSIONS

► First part of my thesis is focused on the fabrication of colloidal gold NPs assembled of different morphologies by using three very simple strategies based on evaporation-induced assembly (i.e. drop-casting and convective self-assembling (CSA)) and chemical functionalization.

The SERS performance of the as-prepared substrates was assessed by analyzing the SERS response of adsorbed p-aminothiophenol (p-ATP), used as Raman reporter, under 532, 633, and 785 nm laser excitation wavelengths. The NPs strips obtained by CSA prove to be the most efficient SERS substrates, active both in the visible and NIR spectral regions, possessing a highly uniform SERS response as demonstrated by spectra at individually selected sites and by confocal SERS mapping.

Finally, we demonstrated that these NPs strips are effective for the detection of cytosine, a DNA component, and for multi-analyte SERS detection. These results, showing how an efficient SERS substrate can be obtained by a very simple assembly method from easy-to-synthesize colloidal gold NPs, can have an impact on the development of analytical SERS applications.

► Subsequently, dual-scale SERS substrates based on periodically microstructured films of colloidal gold NPs were fabricated by binary CSA from a colloidal mixture of 15 nm gold NPs and 500 nm polystyrene (Ps) microspheres.

We offer a clear demonstration of the multiplicative SERS enhancement generated by these substrates inferring the potential impact of our results on the future design of nano- and micro-structured SERS substrates. The multiplicative SERS enhancement effect was evidenced for both internal Raman reporters (molecules attached to the gold NPs before their assembly) and external Raman probes (molecules adsorbed on the samples after NPs film assembly), and was attributed to the superposition of plasmon-enhanced near-fields (due to nano-scale inter-nanoparticle gaps) with far-field diffracted light (due to periodic micro-scale pattern).

Moreover, the ability of the patterned films for far-field light coupling is demonstrated by the measured reflectivity spectra, which present minima/maxima in the visible spectral range, and electric field maps obtained by FDTD simulations. The fabricated dual-scale SERS substrates exhibit a good spot-to-spot reproducibility and remarkable time stability, as proved by analyzing the SERS response over a time scale longer than one month.

► The last part of my thesis presents a cost-effective, simple and rather fast method to fabricate periodically nanostructures by taking advantage of thermal properties of two classes of polymers, namely hydrogels and thermoplastic. With this approach, we fabricated highly ordered pyramidal-shaped nanostructures using the texture of a commercial DVD as the initial mold.

Additionally, we demonstrate the SERS efficiency of the fabricated structure to detect urea molecules found in the fingerprint. Moreover, due to the periodicity of the pyramidal-shaped structures, the obtained substrate can be successfully employed to correlate the intensity of the specific SERS peak of urea with the molecules concentration to obtain a calibration curve. Considering that the concentration of urea can be used as a marker for kidney injuries, the fabricated substrate shows promise for the development of lab-on-a-chip devices for early detection of kidney diseases. In conclusion, the pyramidal-shaped substrate fabricated through this cost-effective method, could be successfully used for the development of a quantitative SERS renal sensor.

REFERENCES

- Aslan, K., Gryczynski, I., Malicka, J., Matveeva, E., Lakowicz, J.R., and Geddes, C.D. (2005). *Curr. Opin. Biotechnol.* 16, 55–62
- Baia, M., Toderas, F., Baia, L., Maniu, D., and Astilean, S. (2009). *ChemPhysChem* 10, 1106–1111.
- Bunzendahl, M., Lee-Van Schaick, P., Conroy, J.F.T., Daitch, C.E., and Norris, P.M. (2001). *Colloids Surf. Physicochem. Eng. Asp.* 182, 275–283.
- Coe, J.V., Heer, J.M., Teeters-Kennedy, S., Tian, H., and Rodriguez, K.R. (2008). *Annu. Rev. Phys. Chem.* 59, 179–202.
- Cole, R.M., Baumberg, J.J., Garcia de Abajo, F.J., Mahajan, S., Abdelsalam, M., and Bartlett, P.N. (2007). *Nano Lett.* 7, 2094–2100.
- Deegan, R.D., Bakajin, O., Dupont, T.F., Huber, G., Nagel, S.R., and Witten, T.A. (1997). *Nature* 389, 827–829.
- Dimitrov, A.S., and Nagayama, K. (1996). *Langmuir* 12, 1303–1311.
- Ding, T., Song, K., Clays, K., and Tung, C.-H. (2009). *Adv. Mater.* 21, 1936–1940.
- Farcau, C., Moreira, H., Viallet, B., Grisolia, J., and Ressier, L. (2010). *ACS Nano* 4, 7275–7282.
- Grisolia, J., Viallet, B., Amiens, C., Baster, S., Cordan, A.S., Leroy, Y., Soldano, C., Brugger, J., and Ressier, L. (2009). *Nanotechnology* 20, 355303.
- Hall, D. (2001). *Anal. Biochem.* 288, 109–125
- Haynes, C.L., and Van Duyne, R.P. (2001). *J. Phys. Chem. B* 105, 5599–5611.
- Jensen, T.R., Malinsky, M.D., Haynes, C.L., and Van Duyne, R.P. (2000). *J. Phys. Chem. B* 104, 10549–10556.
- Kelf, T.A., Sugawara, Y., Cole, R.M., Baumberg, J.J., Abdelsalam, M.E., Cintra, S., Mahajan, S., Russell, A.E., and Bartlett, P.N. (2006). *Phys. Rev. B* 74, 245415.
- Keuleers, R., Desseyn, H.O., Rousseau, B., and Van Alsenoy, C. (1999). *J. Phys. Chem. A* 103, 4621–4630.

- Kreibig, P.D.U., and Vollmer, P.D.M. (1995). Introduction. In *Optical Properties of Metal Clusters*, (Springer Berlin Heidelberg), pp. 1–12.
- Kretschmann, E., and Raether, H. (1968). *Z Naturf* 23 A, 2135.
- Lee, J.A., Reibel, K., Snyder, M.A., Scriven, L.E., and Tsapatsis, M. (2009). *ChemPhysChem* 10, 2116–2122.
- Liu, G.L., Yin, Y., Kunchakarra, S., Mukherjee, B., Gerion, D., Jett, S.D., Bear, D.G., Gray, J.W., Alivisatos, A.P., Lee, L.P., et al. (2006). *Nat. Nanotechnol.* 1, 47–52.
- Makiabadi, T., Bouvrée, A., Nader, V.L., Terrisse, H., and Louarn, G. (2010). *Plasmonics* 5, 21–29.
- McCreery, R.L. (2000). *Raman Spectroscopy for Chemical Analysis*. In *Raman Spectroscopy for Chemical Analysis*, (John Wiley & Sons, Inc.),.
- Michaels, A.M., Nirmal, M., and Brus, L.E. (1999).. *J. Am. Chem. Soc.* 121, 9932–9939.
- Neil, E., Peter, G., and John, C. (2007). *Vibrational Spectroscopy of Polymers: Principles and Practice* (Willey).
- Noginov, M.A., Vondrova, M., Williams, S.N., Bahoura, M., Gavrilenko, V.I., Black, S.M., Drachev, V.P., Shalaev, V.M., and Sykes, A. (2005). *J. Opt. Pure Appl. Opt.* 7, S219.
- Otto, A. (1968). *Z. Für Phys.* 216, 398–410
- Park, J.-S., Park, J.-W., and Ruckenstein, E. (2001).. *Polymer* 42, 4271–4280.
- Prevo, B.G., Hwang, Y., and Velev, O.D. (2005). *Chem. Mater.* 17, 3642–3651.
- Raether, H. (1988). Introduction. In *Surface Plasmons on Smooth and Rough Surfaces and on Gratings*, (Springer Berlin Heidelberg), pp. 1–3
- Rossi, R.C., Tan, M.X., and Lewis, N.S. (2000). *Appl. Phys. Lett.* 77, 2698–2700.
- Sánchez-Cortés, S., and García-Ramos, J.V. (2001). *Surf. Sci.* 473, 133–142.
- Schuck, P. (1997). *Annu. Rev. Biophys. Biomol. Struct.* 26, 541–566.
- Toderas, F., Baia, M., Baia, L., and Astilean, S. (2007). *Nanotechnology* 18, 255702.
- Turner, A.P.F. (2000). *Biosensors--Sense and Sensitivity. Science* 290, 1315–1317.
- Updike, S.J., and Hicks, G.P. (1967). The enzyme electrode. *Nature* 214, 986–988.
- Vogel, E., Gbureck, A., and Kiefer, W. (2000). *J. Mol. Struct.* 550–551, 177–190.
- Watanabe, S., Inukai, K., Mizuta, S., and Miyahara, M.T. (2009). *Langmuir* 25, 7287–7295.
- Whitesides, G.M.; Love, J.C. (2001) *Sci. Am.* 285, 32 – 41.
- Xu, J., Xia, J., Hong, S.W., Lin, Z., Qiu, F., and Yang, Y. (2006).. *Phys. Rev. Lett.* 96, 066104.
- Yguerabide, J., and Yguerabide, E.E. (1998). *Anal. Biochem.* 262, 157–176.
- Yuan, Z., Burckel, D.B., Atanassov, P., and Fan, H. (2006). *J. Mater. Chem.* 16, 4637–4641.
- Zhang, X., Yonzon, C.R., and Van Duyne, R.P. (2006). *J. Mater. Res.* 21, 1083–1092.

LIST OF PUBLICATIONS

Related to thesis (ISI)

C. Leordean, M. Potara, S. Boca-Farcau, A. Vulpoi, S. Astilean and C. Farcau, Multiscale electromagnetic SERS enhancement on self-assembled micropatterned gold nanoparticle films, **J. Raman Spectrosc.** **45** (2014) 627-635.

C. Leordean, A. M. Gabudean, V. Canpean and S. Astilean, Easy and cheap fabrication of ordered pyramidalshaped plasmonic substrates for detection and quantitative analysis using surface-enhanced Raman spectroscopy, **Analyst** **138** (2013) 4975-4981.

C. Leordean, V. Canpean and S. Astilean, Surface-Enhanced Raman Scattering (SERS) Analysis of Urea Trace in Urine, Fingerprint, and Tear Samples, **Spectrosc. Lett.** **45** (2012) 550-555.

C. Farcau, M. Potara, **C. Leordean**, S. Boca, S. Astilean, Reliable plasmonic substrates for bioanalytical SERS applications easily prepared by convective assembly of gold nanocolloids, **Analyst** **138** (2013) 546-552.

Unrelated to thesis (ISI)

I. Botiz, P. Freyberg, **C. Leordean**, A.M. Gabudean, S. Astilean, A. C.M. Yang, N. Stingelin Emission properties of MEH-PPV in thin films simultaneously illuminated and annealed at different temperatures, **Synt. Met.** 10.1016/j.synthmet.2014.10.031 (2014)

I. Botiz, P. Freyberg, **C. Leordean**, A.-M. Gabudean, S. Astilean, A. C.-M. Yang, N. Stingelin, Enhancing the Photoluminescence Emission of Conjugated MEH-PPV by Light Processing, **ACS Appl. Mater. Interfaces** **6** (2014) 4974–4979.

M. Iliut, **C. Leordean**, V. Canpean, C. M. Teodorescu and S. Astilean, A new green, ascorbic acid-assisted method for versatile synthesis of Au–graphene hybrids as efficient surface-enhanced Raman scattering platforms, **J. Mater. Chem. C** **1** (2013) 4094-4104.

M. Iliut, A. M. Gabudean, **C. Leordean**, T. Simon, C. M. Teodorescu, S. Astilean, Riboflavin enhanced fluorescence of highly reduced graphene oxide, **Chem. Phys. Lett.** **586** (2013) 127–131.